Journal of Structural Geology, Vol. 15, No. 11, pp. 1273 to 1292, 1993
Printed in Great Britain

0191-8141/93 $06.00+0.00

Evaluation of upper mantle microstructures in the Table Mountain massif (Bay of Islands ophiolite)

GÜNTER SUHR*

Department of Earth Sciences, Memorial University of Newfoundland, St. John's, Newfoundland, Canada A1B 3X5

(*Received* 4 *March* 1992; *accepted in revised form* 31 *October* 1992)

Abstract—Within the undisrupted, 6 km thick mantle section of the Table Mountain massif (Bay of Islands ophiolite, Newfoundland), several distinct peridotite microstructures are recognized. In the uppermost mantle section, very high temperature ($T \sim 1200°$), high strain microstructures with evidence for syntectonic melt infiltration are preserved. Remarkable among these is an orthopyroxene-impregnated dunite. At an intermediate level of the mantle section, peridotites have been affected by a weak, lower temperature ($T = 1000$–$1100°C$) overprint. They are underlain by a thin sliver of low strain, high temperature peridotites. All these peridotites are interpreted to have formed during spreading-related strain. Lower temperature ($T < 1000°C$), high stress microstructures with high accumulated strain are locally preserved at intermediate levels of the mantle section and are regionally present at its base. They culminate in (metasomatic) ultramafic ultramylonites and are related to detachment of the ophiolite.

With the exception of the basal ultramylonitic peridotites, the activated olivine slip system was (0*kl*)[100]. In the highest temperature peridotites, a weak preference for the activation of distinct slip planes ((010),(001),(011)) was noted. Based on piezometry and olivine flow laws, strain rate estimates for the basal detachment fabrics are $10^{-12}\,s^{-1}$. This strain rate is consistent with the observed width of detachment overprint in the ophiolite and reasonable plate tectonic convergence rates. Strain rate estimates for the very high temperature peridotites are even higher. Recent data about grain growth rates in olivine indicate that, in order to preserve the peridotite microstructures, olivine grain growth must have been highly impeded. Olivine flow law data suggest that even peridotites with lower temperature microstructures ($T \geq 900$–$950°C$) could form within the rheological asthenosphere. The detachment or spreading-related origin of peridotites with a lower temperature overprint may thus only be concluded from the regional geological context.

INTRODUCTION

THE microstructures of upper mantle xenoliths have been classified by Mercier & Nicolas (1975). Their nomenclature has been supplemented or modified several times (Boullier & Nicolas 1975, Harte 1977, Pike & Schwarzman 1977, Mercier 1985) but little has changed in the original concept. A relatively undeformed microstructure (protogranular, coarse, granoblastic, allotriomorphic granular) was distinguished from a moderately deformed one (porphyroclastic, heteroblastic) and a highly deformed microstructure (fine-grained equigranular, granuloblastic). Less common microstructures include a poikiloblastic texture (Mercier 1985), fluidal textures inferred to form by superplastic flow (Boullier & Gueguen 1975) and secondary textures (annealed, protogranular II) (Mercier & Nicolas 1975, Mercier 1985).

In addition to the occurrence as xenoliths in basaltic rocks, fragments of upper mantle peridotites are accessible on continents as km-scale exposures in the structurally lower portion of many ophiolites and in orogenic lherzolites. The application of the xenolith-based classification of peridotite microstructures to mantle peridotites from ophiolites is, however, difficult. Ophiolitic peridotites have suffered a flow history distinctly different from that of mantle xenoliths. During their long deformational history, the ophiolitic mantle peridotites were brought up from depth to shallow levels beneath an oceanic spreading centre. This ascent along an oceanic geotherm was followed typically, but not necessarily, cf. diapiric structures preserved in the Oman ophiolite (Ceuleneer *et al.* 1988), by subhorizontal flow at rapidly decreasing temperatures away from, or parallel to, the ridge. Subsequently, the structurally lower portion of many ophiolites (i.e. the mantle rocks) has been affected by plastic deformation related to lithospheric decoupling during the initiation of ophiolite obduction. Considering this complex flow history, it is not surprising that true protogranular microstructures are extremely rare or not seen in ophiolitic peridotites. Nevertheless, Mercier (1985) has proposed a classification comprising both peridotites in xenoliths and massifs. The unique situation of ophiolitic peridotites was accounted for in the classifications of Nicolas *et al.* (1980), Nicolas (1986a) and Ceuleneer *et al.* (1988). In the latter papers, the terms asthenospheric microstructure and lithospheric microstructure were introduced.

The asthenospheric microstructure relates to very high temperature, low stress deformational conditions. It is restricted to coarse-grained olivine microstructures, either characterized by a coarse, unimodal (Ceuleneer *et al.* 1988) or bimodal (Nicolas 1986a) olivine grain size. Optical extinction is flat, resulting in sharply defined grain boundaries. In contrast to the protogranular structure of xenoliths, the olivine lattice fabric is exceptionally strong. Features indicative of melt-impregnation are

*Current address: Mineralogisch Petrographisches Institut, Universität zu Köln, Zülpicher Strasse 49, D-5000 Köln 1, Germany.

often, though not necessarily, associated with asthenospheric microstructures. The asthenospheric microstructure was assigned to the spreading period of ophiolitic peridotites.

The lithospheric microstructure is characterized by fine-grained olivine neoblasts reflecting lower temperature, higher deviatoric stress conditions if compared to the asthenospheric peridotites. Typical are tightly spaced tilt walls (optical subgrain boundaries) and/or abundant undulose extinction indicative of less effective recovery. Neoblasts and thus a porphyroclastic texture develop from a coarse texture only after an appreciable (>40%) amount of lithospheric strain (Nicolas 1978, Karato *et al.* 1980, 1982, Karato 1984). Peridotites with a weak overprint of lithospheric strain may thus still have a coarse, unimodal grain size with, however, a tighter olivine substructure (Ceuleneer *et al.* 1988). Significant lithospheric strain is assigned to detachment tectonics and results in mylonitic textures (Nicolas *et al.* 1980, Nicolas 1986a).

A consistent point of criticism in this classification has been the global geophysical implications of the terms 'lithospheric' and 'asthenospheric'. As shown in this paper, such implications are often difficult to justify and may even be wrong in some cases. The classification into the two groups will be retained, as it is considered powerful for descriptive purposes. However, the two groups are here referred to, less elegantly and deviating from their earlier usage (Suhr 1992), as 'very high temperature microstructures' (asthenospheric) and 'lower temperature microstructures' (lithospheric).

This paper documents the microstructural variation within one of the four massifs of the Bay of Islands ophiolite, Newfoundland. The temperatures of deformation are estimated and strain rates are assigned by using stress estimates and olivine flow laws. Problems related to the preservation of the microstructures are discussed and the spreading or detachment-related origin of lower temperature ('lithospheric') microstructures is evaluated.

GEOLOGICAL OUTLINE

The Lower Ordovician Bay of Islands ophiolite forms the highest structural slice of the Humber Arm Allochthon in western Newfoundland (Williams 1973, 1975, Williams & Cawood 1989). It is subdivided into the Coastal Complex and Bay of Islands Complex (BOIC) (Fig. 1) of which only the latter preserves a classical ophiolite stratigraphy (Karson & Dewey 1978). The BOIC is exposed in four massifs, all of which expose a moderately W-dipping boundary between upper mantle rocks (harzburgites and less common lherzolites) and dunites, wehrlites and gabbros. This boundary presumably represents the ancient petrologic Moho and as such is assumed to have been regionally subhorizontal before the massifs were folded during later obduction. Amphibolites and lower grade metamorphic rocks (typically metavolcanics) form the metamorphic sole (Figs. 1 and 2). The sole was accreted to the base of the detached ophiolite during early obduction of the ophiolite.

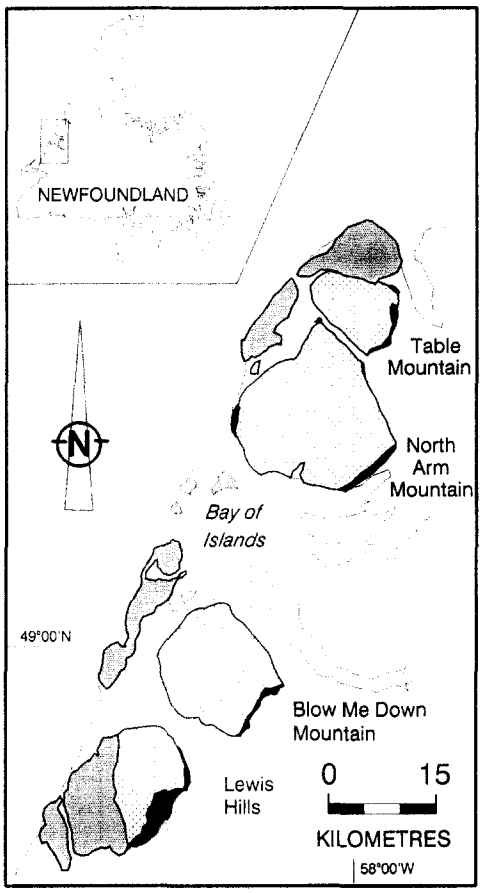

Fig. 1. Location of the Bay of Islands ophiolite. Stippled area—Bay of Islands Complex; dark shading—Coastal Complex; black—lithologies accreted to the base of the ophiolite during obduction.

The Table Mountain massif (TM, Fig. 2) is tightly folded with crustal gabbros forming the core of a syncline. Higher level oceanic rocks, preserved in the two massifs to the south of TM, were eroded off TM. The mantle sequence from the oceanic Moho to the metamorphic sole is preserved within the eastern limb of the syncline in TM (Girardeau & Nicolas 1981) (Fig. 2). The thickness of the mantle section is measured as distance normal to the Moho. In Table Mountain, this thickness is 6–7.5 km, depending on the exact current dip of the Moho (45° or 60°, respectively).

The top of the investigated section in TM is formed by massive dunites of variable thickness with minor (plagioclase–) wehrlite layers. Below, fine-grained, clinopyroxene-rich harzburgites are encountered. The abundance of clinopyroxene decreases very gradually down-section where fairly monotonous, clinopyroxene-poor harzburgites dominate. Coarse-grained lherzolites are abundant at the base of the mantle sequence and are present in all four massifs (Church & Riccio 1977, Malpas 1978).

On a structural basis, the mantle sequence (including the massive dunites) in the TM massif can be divided into six units which are assigned to specific tectonic events (Suhr 1992) (Fig. 2). Structural unit boundaries

are marked by changes in the orientation of the high temperature mineral stretching lineation. Four of the structural units reflect the progressive evolution of the spreading-related mantle flow pattern as the TM massif was carried away from the ridge axis. Suhr (1992) suggested an evolution from ridge parallel flow (unit 1) to plate driven flow (unit 2) and forced flow (unit 3). Conclusions about the driving forces of the flow are derived from microstructurally determined shear senses together with the reconstructed position of the paleoridge. The latest spreading-related history preserved in TM could relate to the underplating of an off-axis diapir (unit 5). This evolution is seen as one occurring during the final stages of a spreading centre. Unit 6 and probably also unit 4 formed later during detachment of the ophiolite. A variable, structurally gradational region between units 4 and 5 was assigned to a transitional unit.

MICROSTRUCTURES OF THE TABLE MOUNTAIN MANTLE SECTION

For each of the six structural units, the most characteristic microstructures are presented as *type microstructures*. The numbers given to the type microstructures refer to the structural unit in which they occur. Locations of the illustrated samples are given in Fig. 2. A type microstructure may not be the most common microstructure within a unit. It is, however, thought to represent peridotite microstructures which have suffered minimal overprint associated with deformation of another unit. The microstructural variations and trends within each unit, in addition to the type microstructure, are briefly discussed. It is emphasized that the microstructural changes along structural unit boundaries are not abrupt but gradational. All microstructural observations and drawings are made from thin sections cut perpendicular to the foliation and parallel to the mineral stretching lineation. Stress estimates are derived from the average neoblast size of olivine using the calibration of Karato *et al.* (1980). This calibration was performed during conditions of subgrain rotation as the preferred mechanism of recrystallization. Subgrain rotation is thought to dominate over grain boundary migration unless stresses are very high (Nicolas 1978). According to Karato *et al.* (1982), the neoblast size established during migration recrystallization might not be very different from that formed during rotation recrystallization. The piezometer of Karato *et al.* (1980) yields lower stress values for a given neoblast size than the calibrations of Mercier *et al.* (1977), Post (1977) and Ross *et al.* (1980).

Type microstructure 1: *orthopyroxene-impregnated dunite*

This interesting sample (TM 1315) is located in the transition from massive dunites to harzburgites. This zone also constitutes the transition from ridge-parallel (unit 1) to ridge-normal flow (unit 2, see Fig. 2).

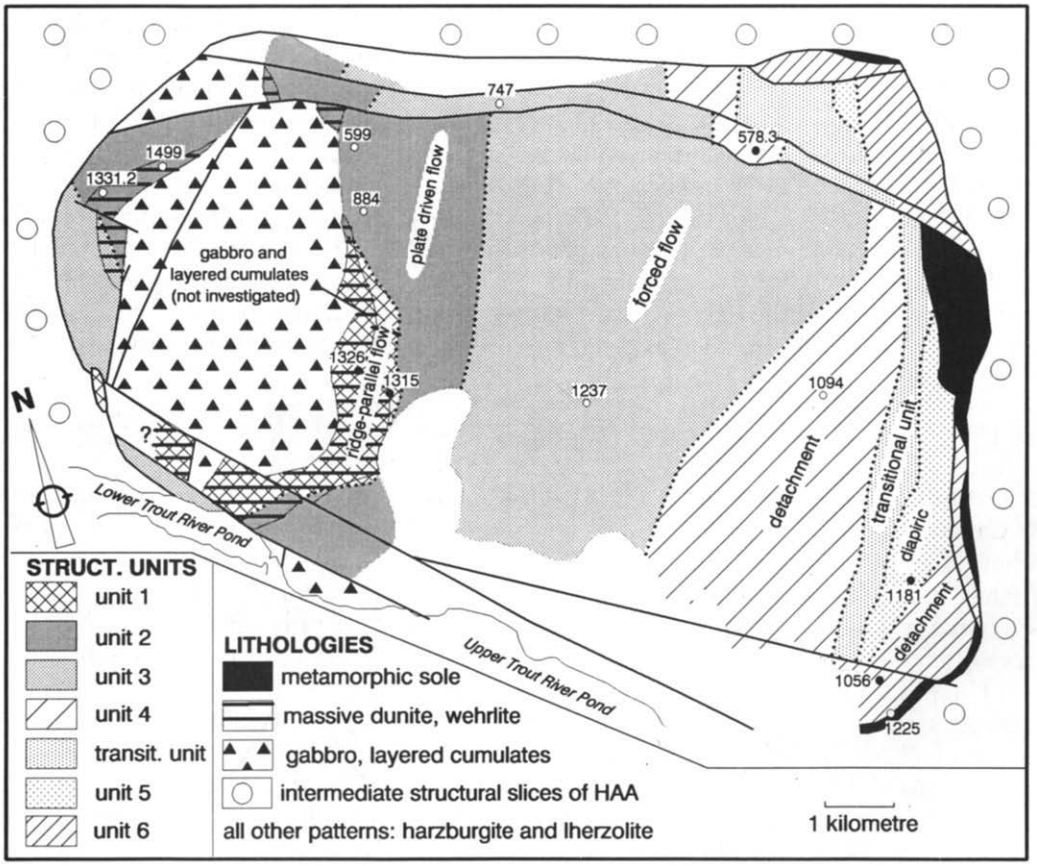

Fig. 2. Structural units in the Table Mountain massif and main lithological boundaries. Numbers indicate location of illustrated samples. HAA—Humber Arm Allochthon.

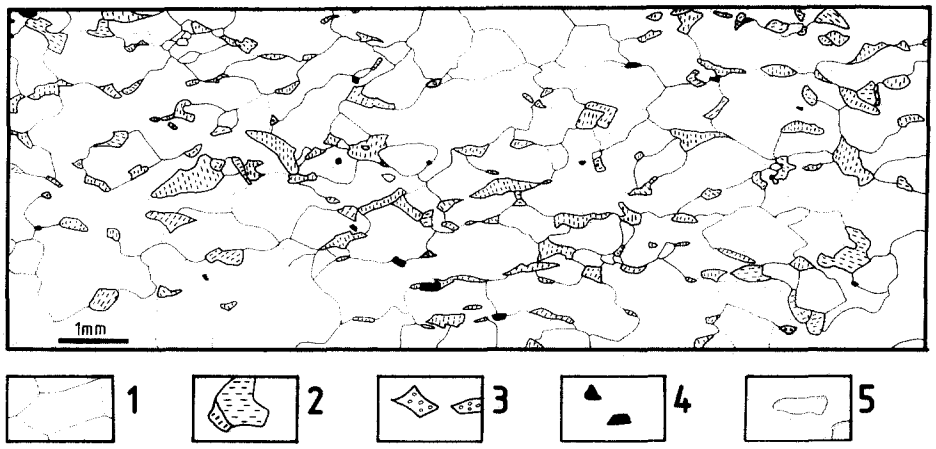

Fig. 3. Line drawing of type microstructure 1 (TM 1315), representing a high strain, orthopyroxene-impregnated dunite. For all line drawings, the following patterns apply. 1—olivine, with tilt walls; 2—orthopyroxene, dashes parallel to cleavage trace; 3—clinopyroxene; 4—spinel; 5—plagioclase (internal structure not visible due to alteration). Foliation trace is always parallel to scale bar.

In Fig. 3 the unimodal microstructure of olivine is shown. Olivine grains are well recovered and weakly flattened. In the orthopyroxene-poor part of the sample (not shown), the olivine structure is less flattened and still coarser, suggesting that the shape of the olivine grains is partly controlled by the distribution of elongated orthopyroxene grains. Local enclosure of orthopyroxene by olivine suggests migration of olivine grains boundaries. The preferred orientation of olivine is strong in the sample (gypsum plate test). Spinels are very small and sub-to euhedral or weakly elongated. Clinopyroxene occurs as very rare interstitial grains in the same habit as orthopyroxene.

Orthopyroxene forms elongated, attenuated, flaser-like grains which are well aligned (Fig. 3) (see also fig. 3a in Suhr & Robinson 1993). Most of the traces of the cleavage (100) of orthopyroxene are perpendicular to the foliation. This is peculiar as it implies that the orthopyroxene slip plane (100) is also oriented at high angle to the foliation. It would preclude that orthopyroxene has undergone a significant overprint by dislocation glide on the well established slip system (100) [001] (Etheridge 1975, Carter 1976, Nicolas & Poirier 1976) or on the less well known system (010) [001] (Nazé *et al.* 1987). An orthopyroxene lattice fabric analysis (Fig. 4) supports these observations: the [001] slip direction lies perpendicular to the foliation and the potential slip plane (100) forms a girdle about the [001] direction, i.e. is always perpendicular to the foliation. Recrystallization is absent in orthopyroxene as can be seen from the lack of subgrains and neoblasts and the preservation of delicate tips of grains.

A formation of orthopyroxene due to corrosion (i.e. residual grains of orthopyroxene) would be favoured from the geological context, i.e. the position of the sample in the transition from residual harzburgite to massive dunite. However, a residual model does not explain the lattice orientation. As the shape fabric resembles documented melt impregnation morphologies (e.g. Nicolas & Dupuy 1984, Evans & Hawkins 1989), a derivation from trapped melt is favoured. Locally, a similar habit of orthopyroxene has been found in harzburgites of units 2 and 3, although the characteristic morphology in these samples is restricted to a few of a large number of orthopyroxene grains. Recently, Cannat *et al.* (1990) have shown lattice orientation data from

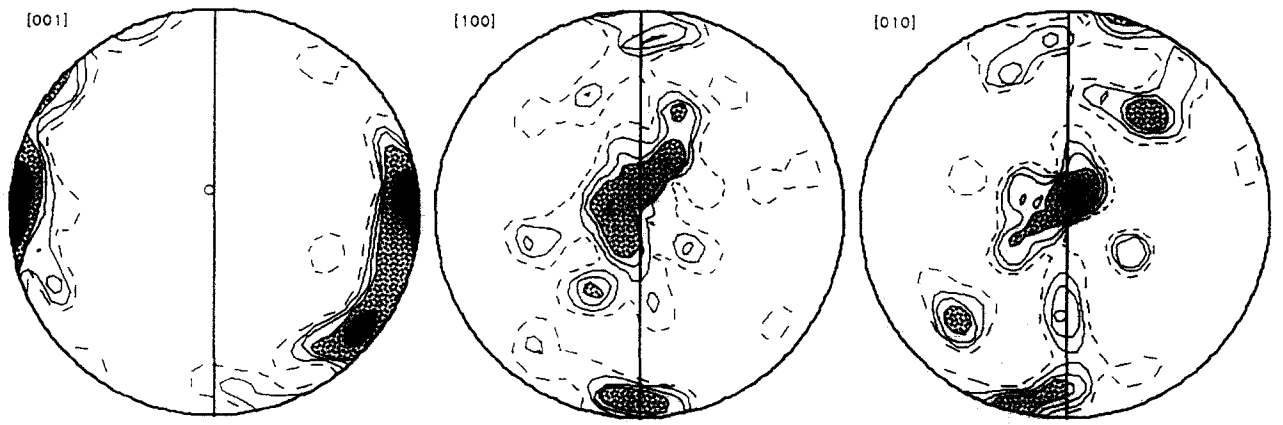

Fig. 4. Stereographic projection (lower-hemisphere, equal-area) of orthopyroxene lattice data. Fifty grains measured; (smoothed) contours at 1,2,3,4,8% per 1% area. Vertical line indicates foliation trace; dots are pole to mineral stretching lineation; sample TM 1315.

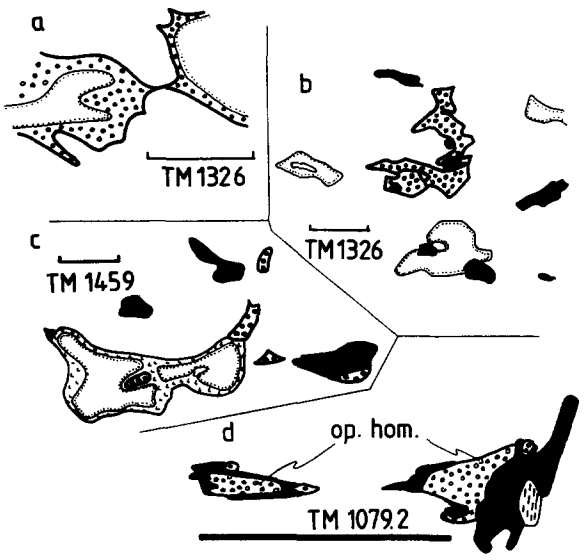

Fig. 5. Microstructural details. Scale bar is 0.5 mm long; for legend see Fig. 3. No grain boundaries are shown for the olivine matrix. (a) Clinopyroxene rimming plagioclase. (b) Clinopyroxene oriented at a high angle to the foliation defined by plagioclase and spinel. (c) Plagioclase with optically continuous rim of pargasite (hook pattern). (d) Spinel–clinopyroxene (and minor orthopyroxene) cluster separated by olivine matrix but showing identical optical extinction of clinopyroxene.

interstitial orthopyroxene grains of abyssal peridotites of the Garret transform fault which are also incompatible with an origin by deformation.

The preferred interpretation of this sample is formation of the orthopyroxene due to crystallization from a melt percolating through dunite during strong deformation. A likely product of the same melts are the abundant orthopyroxenite dykes present in the Table Mountain mantle section. The shape of orthopyroxene grains was potentially controlled by the flow fabric in the dunite. The origin of the orthopyroxene lattice fabric may lie in a few poikilitic orthopyroxene grains.

Further microstructural features of unit 1

Within unit 1, massive dunites range from the type microstructure 2A (discussed further below) to dunites with a bimodal (porphyroclastic) olivine structure. The latter have an average neoblast size in the range of 0.8 mm (corresponding to a deviatoric stress σ_d = 7 MPa, Karato *et al.* 1980). The olivine microstructure is generally well recovered and the lattice fabric appears strong. Inclusion-rich patches and trails in olivine are common. Spinels are fine grained (~0.2 mm) and elongated with aspect ratios of 2–4. Rarely, larger, anhedral to subhedral spinel grains occur.

Within the dunites, rare plagioclase- and clinopyroxene-rich bands occur. In the bands, plagioclase has an interstitial morphology and is elongated. It is nearly always altered to hydrogarnet so that the degree of recrystallization is poorly known. In the few grains where plagioclase is preserved, recrystallization is obvious. Clinopyroxene tends to occur as a partial or complete rim on plagioclase (Fig. 5a) or interstitially within the olivine matrix. The interstitial grains may be elongated at high angles to the foliation (Fig. 5b). This feature was also observed in dunites from the Blow Me Down massif (Fig. 6a). The morphology of clinopyroxene near the olivine matrix is commonly more complex and delicate than the typically well-rounded clinopyroxene–plagioclase interfaces (Fig. 5a). The complex external morphology of clinopyroxene argues against an origin of clinopyroxene by simple reaction of plagioclase with the olivine matrix. The arrangement of clinopyroxene at a high angle to the foliation is similar to so called 'streamers' (e.g. Volker & Upton 1990) inferred to derive from the incomplete extraction of residual melt during matrix compaction, an origin also favoured for the BOIC occurrences. In several samples, a thin, optically continuous rim of amphibole occurs around plagioclase (Fig. 5c) (see also Himmelberg & Loney 1980). It is developed neither around spinel nor clinopyroxene and indicates a reaction between plagioclase and the olivine matrix in the presence of a fluid.

Type microstructure 2A: *very high temperature dunite showing important grain growth*

On the western side of TM, the massive dunites have been affected by ridge-normal flow (structural unit 2). The sample TM 1331.2 of type microstructure 2A is located near the base of this dunite sequence (Fig. 2). The olivine structure is coarse and well recovered with sharp grain boundaries and poor shape fabrics (Fig. 7). Rare tilt walls are well-defined and straight, and grain boundaries are curvilinear. Triple point junctions at 120° and poikilitic enclosure of spinel by olivine are common. A highly deformed state for this sample is suggested by the very strong olivine lattice fabric (Fig. 8a). The lattice fabric indicates activation of the (0*kl*) [100] slip system. Patches and trails of tiny inclusions within olivine, abundant in other dunite samples, are absent in this sample. Probably they have been swept out by the migration of olivine grain boundaries. Grain boundary migration is also suggested by spinel inclusions within olivine. Neoblasts (0.7 mm diameter) occur mostly in the vicinity of spinel grains. Therefore they probably do not reflect a steady-state grain size (Nicolas *et al.* 1980). Given this fact and the evidence for grain boundary migration, no calculation of deviatoric stress is performed in the sample.

Brownish spinel grains are equant to weakly elongated. Rarely, their shape is irregular. Characteristic are numerous, unidentified, equidimensional inclusions in spinel. Tiny clinopyroxene is rare and occurs interstitially in the olivine matrix. The sample represents a typical, very high temperature, low stress microstructure of a deformed (cumulate?) dunite (cf. fig. 4a in Nicolas 1986a).

Type microstructure 2B: *very high temperature, high strain clinopyroxene-impregnated harzburgite*

The most characteristic microstructure of unit 2 is a high strain, high temperature, clinopyroxene-

impregnated harzburgite. It occurs only in the uppermost part of the unit, both on the eastern and western side of the gabbros. In rare cases, wehrlitic and plagioclase lherzolitic bands are developed in harzburgite. The type sample (TM 884 in Fig. 9) displays a typical banded appearance caused by varying amounts of olivine, orthopyroxene and clinopyroxene.

The olivine microstructure is weakly porphyroclastic in olivine-rich layers, and the average neoblast grain size is 0.4 mm, corresponding to $\sigma_d = 13$ MPa. The neoblast abundance is low. Undulose extinction is nearly absent and tilt walls are rare. In the orthopyroxene-rich bands, the olivine microstructure is equigranular. Petrofabric data (Fig. 8b) suggest activation of the (010)[100] and (001)[100] slip systems.

Orthopyroxene occurs as equant grains with slightly convex or straight grain boundaries and an average grain size of 0.6 mm. The grains either cluster as aggregates of several grains with well developed 120° triple point junctions or are scattered in the olivine matrix. A bimodal grain size distribution is not present. All orthopyroxene grains in this sample are considered to be neoblasts. Typical pull-apart morphologies are absent. The neoblasts typically lack any clinopyroxene exsolution lamellae.

Clinopyroxene is common (up to 5%) and occurs as trails of grains or single grains either with a highly irregular morphology (upper right in Fig. 9 and Fig. 10a; also fig. 3b in Suhr & Robinson 1993) typical of melt impregnation or as equant neoblasts. Some annealing of the impregnations can be noted due to the presence of subgrains and segments of straight grain boundaries instead of curved grain boundaries. The average grain size is 0.5 mm. Most clinopyroxene occurs within olivine-rich zones. Clinopyroxene within orthopyroxene-rich zones is more equant and less irregular-shaped. It might have formed by progressive exsolution from large orthopyroxene grains and recrystallization during high temperature deformation.

Brown–red spinel occurs either as equant, sub- to euhedral grains or weakly elongated grains parallel to the general phase layering in the rock. An intricate intergrowth or association with another phase is uncommon in the type sample but has locally been observed in other similar specimens. Figure 9 shows that spinel occurs preferentially in the orthopyroxene-rich layers and is rare in the olivine-rich layers. Such a relationship is, however, not general and many olivine-rich layers have abundant spinel.

Further microstructural features of unit 2

Down-section within the unit, the following trends develop and continue into unit 3: (i) orthopyroxene is less recrystallized and less scattered; (ii) a bimodal orthopyroxene grain size distribution is preserved. Orthopyroxene porphyroclasts may contain clinopyroxene exsolution lamellae; (iii) grains within orthopyroxene aggregates have more irregular outlines; (iv) spinel may be intergrown with orthopyroxene ± clinopyroxene; it is larger and more irregularly shaped; (v) the olivine structure is somewhat blurred; and (vi) clear evidence for trapped melt becomes rare.

Type microstructure 3: *lower strain harzburgite with a weak, lower temperature overprint*

The central part of the mantle section is among the most serpentinized areas of the massif, so the microstructures of units 3 and 4 are generally poorly preserved. The type sample of unit 3 (TM 747, Fig. 11), located in the central part of unit 3, comes from an area where the lithological banding is oblique to the foliation. The foliation in the hand specimen and on bleached surfaces is indicated by orthopyroxene aggregates and spinel trails, and runs E–W in the illustration. Other trails and aggregates occur in orientations oblique to the foliation and the banding, and the sample may represent a complex transitional stage of readjustment of passive and active markers during folding or even reversals of the sense of shear. Folding of the banding is common in the lower part of unit 3.

The sample illustrated shows three typical features for the microstructure of unit 3: (i) a weak, lower temperature overprint of the olivine microstructure; (ii) relatively fine-grained orthopyroxene aggregates in the 1.5–2 mm range; and (iii) spinel intergrowth with orthopyroxene. The high content of clinopyroxene is, however, not typical for the unit. It may derive from attenuated and disintegrated websteritic banding within harzburgite. Alternatively, it could represent annealed clinopyroxene derived from melt infiltration.

In the olivine matrix undulose extinction and tightly spaced tilt walls are common, and it can be difficult to distinguish between grain and subgrain boundaries. The overall appearance of the olivine matrix, particularly when turning the microscope stage, is blurred. The relationship between the mean orientation of the tilt walls and the foliation indicates a top to right (in Fig. 11) sense of shear. The average neoblast size of 0.25 mm translates into a deviatoric stress of ~20 MPa. Fluid or solid inclusions within olivine are absent.

Orthopyroxene displays a porphyroclastic habit with a few larger porphyroclasts (2 mm) and variably scattered smaller grains (0.4 – 0.8 mm). The grains are less equant than in type microstructure 2B. Several grains have their long axes perpendicular to the lithological banding. They are considered pull-aparts (Darot & Boudier 1975, Suhr *et al.* 1991). The preferred cleavage orientation is poor.

Clinopyroxene ranges from small interstitial grains to large (1.5 mm) grains. It occurs mainly in the olivine matrix, but a few grains share faces with orthopyroxene. An alignment parallel to the lithological banding is present. Deep red spinel occurs intergrown with orthopyroxene.

Further microstructural features of unit 3

In unit 3, olivine grains range from 0.2 to 4 mm, making it difficult to recognize two distinct generations

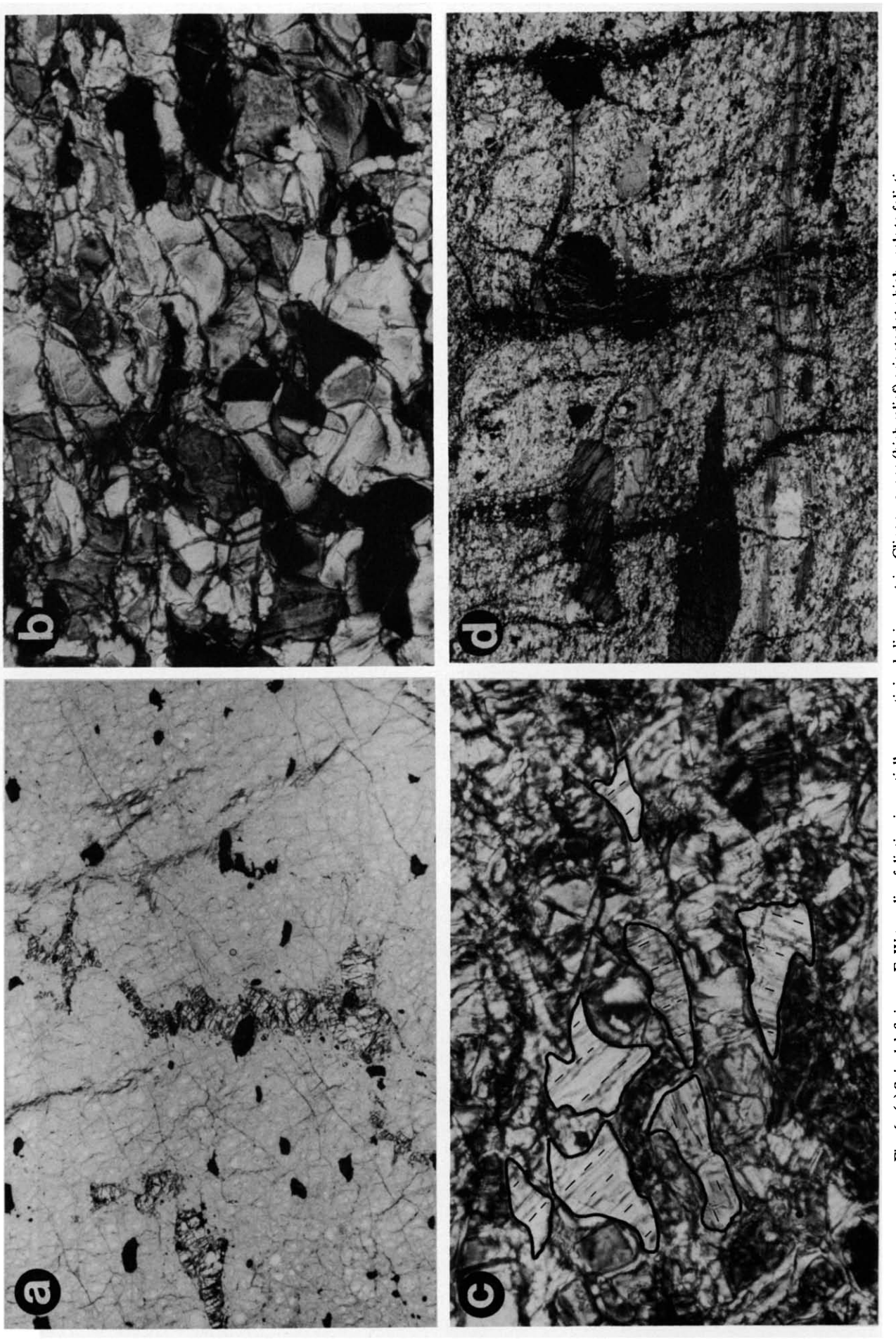

Fig. 6. (a) Spinel defining an E–W-trending foliation in partially serpentinized olivine matrix. Clinopyroxene (high relief) oriented at a high angle to foliation. Sample from massive dunites in the Blow Me Down Massif; long side of photograph is 11.5 mm. (b) Tabular equigranular texture defined by olivine and orthopyroxene. Sample from the high strain zone of unit 4 (TM 1094); long side of photograph is 0.7 mm. (c) Orthopyroxene 'shards' (marked with heavy black lines) in the high strain zone of unit 4 (TM 578.3). Note the orientation of the cleavage trace (marked with thin dashes) at a high angle to the foliation; long side of photograph is 0.7 mm. (d) Mylonitic peridotite with orthopyroxene ribbon grains (e.g. at bottom) and fine-grained olivine matrix (TM 1056); long side of photograph is 11 mm.

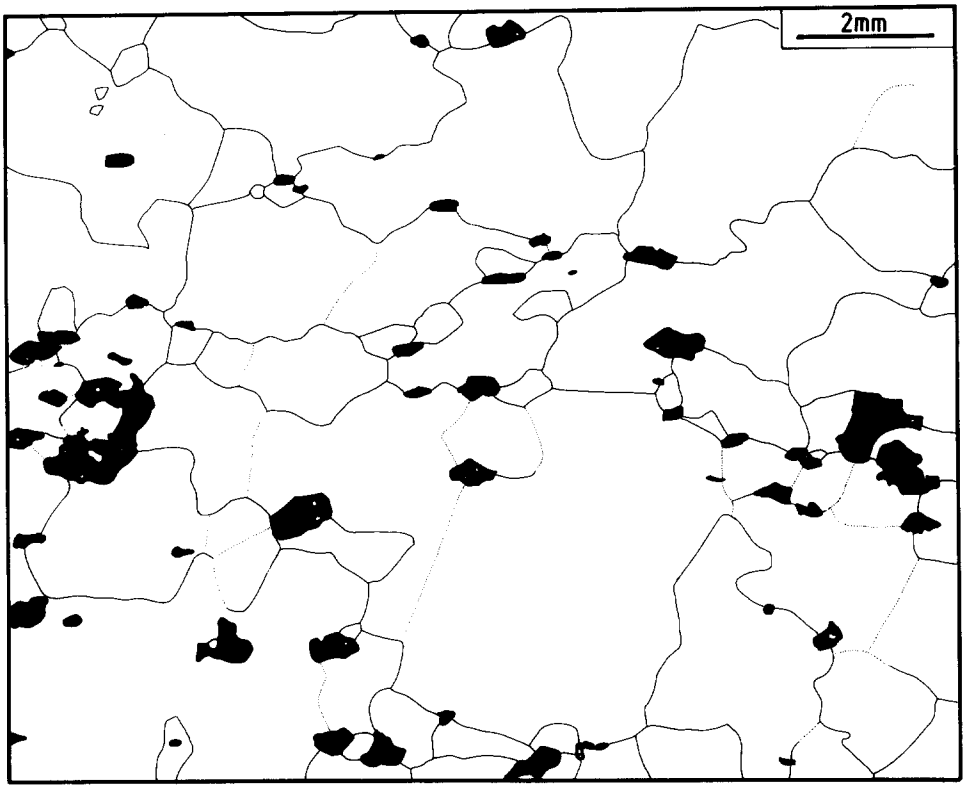

Fig. 7. Line drawing of type microstructure 2A (TM 1331.2), representing a very high temperature, low stress dunite with evidence for important grain boundary migration. For legend see Fig. 3.

of grains (porphyroclasts and neoblasts). In the upper part of unit 3, the transition towards the microstructures typical for unit 2 sets in (see previous section). In particular the progressive disintegration of spinel–orthopyroxene intergrowth textures can be seen (Fig. 10b). In the lower part of unit 3, strain concentrations in the peridotites are seen in the field as sudden deflections of the lithological banding and dykes. Microstructurally, these zones of higher strain are distinct only in a higher degree of scattering of the orthopyroxenes. Overall, pull-apart of orthopyroxene is very common and contributes to the poor shape fabric.

Type microstructure 4: *mylonitic, depleted harzburgite*

Within unit 4, numerous mylonitic high strain zones occur within host harzburgites showing microstructures very similar to those of unit 3. The boundaries of the high strain zones are subparallel to the shape fabric of the host rocks. The sample selected as type microstructure (TM 578.3) represents one of the mylonitic high strain zones.

The olivine microstructure is porphyroclastic in orthopyroxene-poor areas and tabular equigranular in orthopyroxene-rich areas (Fig. 6b). The abundant olivine neoblasts have a size of ~100 μm, corresponding to 42 MPa. Porphyroclasts are often ribbon-shaped with aspect ratios of 3:1–5:1. Micron-sized inclusions can locally be observed in the porphyroclasts. The lattice fabric (Fig. 8c) shows a very strong maximum concentration of the (100) plane, slightly oblique to the mineral lineation. The activated slip system was (0*kl*)[100].

Orthopyroxene aggregates are rare. Most large orthopyroxene grains occur as unrecrystallized, 0.5–2 mm large, rounded porphyroclasts. Very rarely, these grains have undergone moderate slip (aspect ratios <2:1). Part or all of the margins of orthopyroxene porphyroclasts may be recrystallized into a fine-grained mosaic of olivine and orthopyroxene with an average grain size of 50–100 μm.

Characteristic of the high strain samples are shard-like orthopyroxene grains, elongated parallel to the foliation and with the (100) cleavage perpendicular to the foliation and elongation ('hard' orientation) (Fig. 6c). This implies an orientation incompatible with activation of the orthopyroxene slip system (100)[001]). The average size of the shards is 150 × 60 μm. They occur locally in discontinuous bands or as tails to orthopyroxene porphyroclasts, or, as in the type sample, the grains are dispersed throughout the olivine matrix. Where the shards are associated with porphyroclasts they taper out within a short distance of the porphyroclasts, suggesting a genetic relationship with the porphyroclast. The shards remain in their 'hard' orientation for activation of glide even if the associated orthopyroxene porphyroclast has an orientation favourable for dislocation glide. Their formation is poorly understood.

Clinopyroxene is very rare. It occurs as tiny (50–100 μm), elongated, interstitial grains in the olivine matrix parallel to the foliation. It can occur in a habit similar to the orthopyroxene shards. Black or red spinel

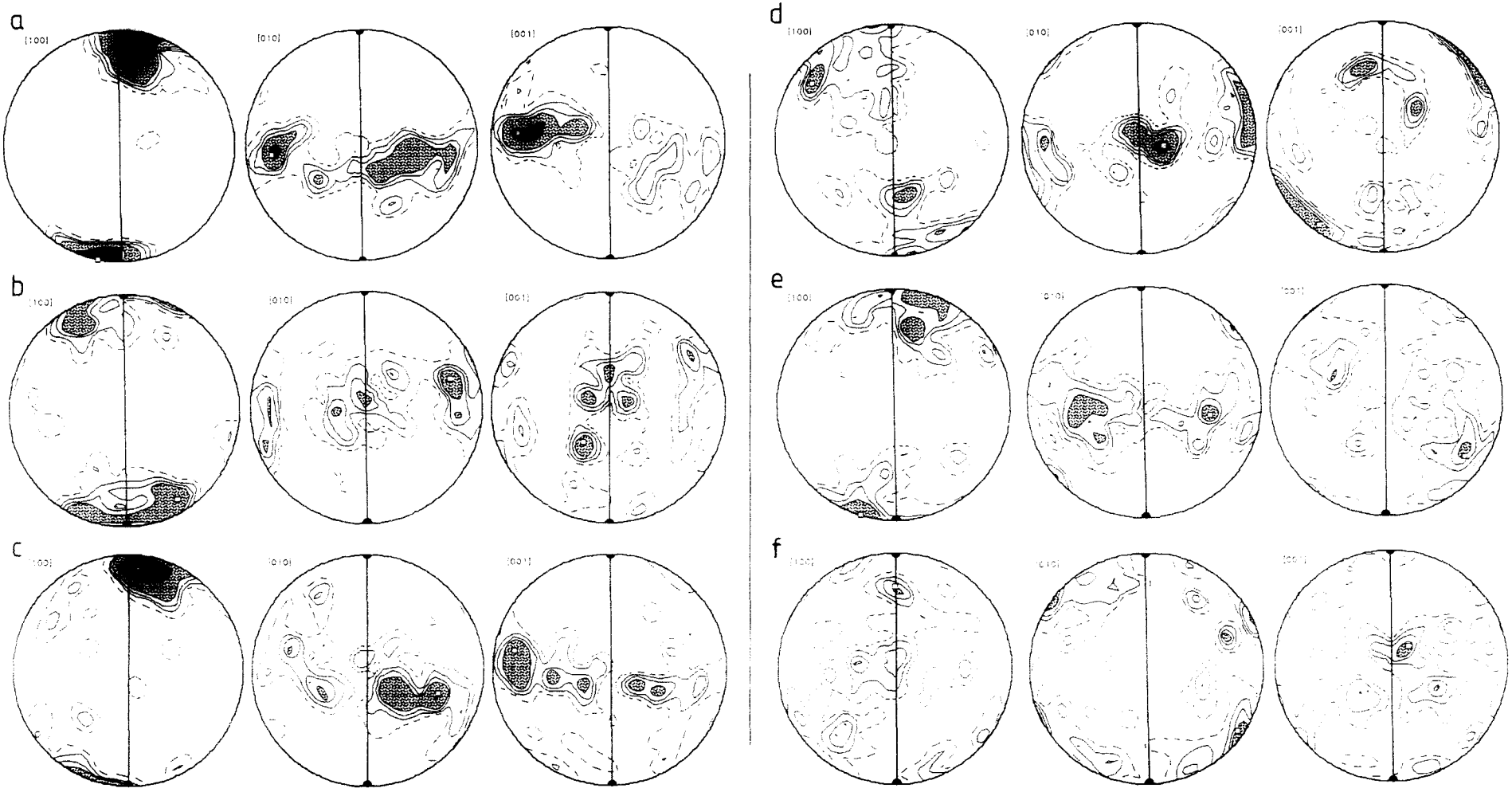

Fig. 8. Stereographic projection of poles to olivine lattice orientations; 100 grains measured in each sample: see Fig. 4 for legend. (a) TM 1331.2. (b) TM 884. (c) TM 578.3. (d) TM 1181. (e) TM 1062. (f) TM 1225.

Fig. 9. Line drawing of type microstructure 2B (TM 884), representing a high strain, very high temperature, clinopyroxene impregnated harzburgite. For legend see Fig. 3.

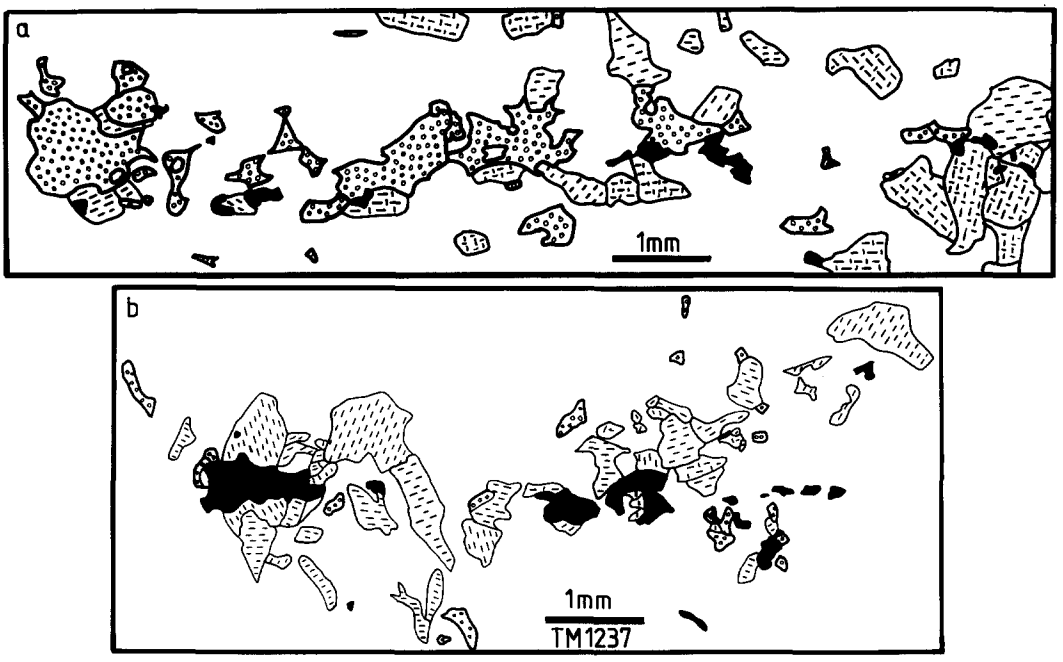

Fig. 10. (a) Enrichment of clinopyroxene in band parallel to the foliation plane in sample TM 599. (b) Disintegration of an orthopyroxene–spinel cluster; olivine grain boundaries are not shown. For legend see Fig. 3.

shows no preferred association with another phase and occurs as scattered, anhedral to euhedral, 15 μm large grains. Large spinel grains up to 1 mm are, however, locally present.

Further microstructural features of unit 4

In several more highly strained samples, good oblique olivine shape fabrics are developed (Drury *et al.* 1990, van der Wal *et al.* 1992). In such fabrics, the shape preferred orientation of olivine is oblique to the foliation defined by spinel and pyroxene grains. The asymmetry of the oblique shape fabrics indicate the same sense of shear as the one derived from asymmetry of the olivine tilt walls (Nicolas & Poirier 1976) and from field evidence.

There is a general tendency for larger orthopyroxene grains to show evidence for slip (i.e. a grain elongation subparallel to the cleavage trace) more frequently than small orthopyroxene grains. As is obvious in peridotites of unit 6 (see below), stress concentrations occur around orthopyroxene grains with an orientation unfavourable for slip. Such high stresses probably resulted in slip of large orthopyroxenes, whereas for small grains deformation was partitioned around the grains.

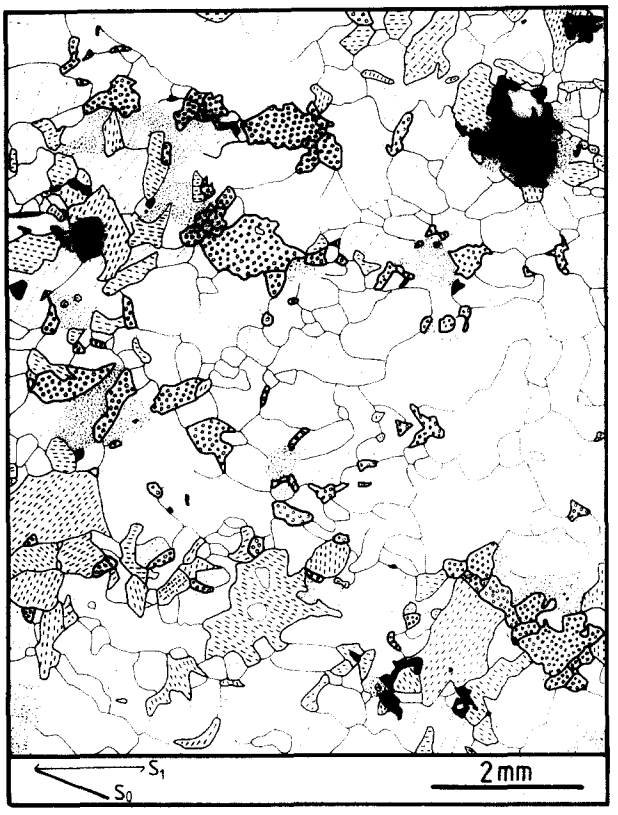

Fig. 11. Line drawing of type microstructure 3 (TM 747), representing a harzburgite with a weak, lower temperature overprint. For legend see Fig. 3.

Type microstructure 5: *coarse, low strain, very high temperature clinopyroxene-impregnated harzburgite*

The most characteristic microstructures are preserved near the base of unit 5. They display a very poor shape fabric of all constituent phases. In particular, the definition of the shape fabric using the spinel orientation is not possible even in bleached hand specimens due to a lack of any spinel preferred orientation (Fig. 12).

The olivine microstructure of sample TM 1181 is weakly porphyroclastic and grains show a typically flat extinction with sharply defined grain boundaries. The neoblast grain sizes range between 0.5 and 1 mm, corresponding to σ_d = 11–6 MPa. The ratio of neoblasts to porphyroclasts is low to moderate. The olivine lattice fabric is only moderately strong, and suggests slip on (010) and (001) in the [100] direction (Fig. 8d). The [100] direction forms, however, an unusual partial girdle in the foliation.

Orthopyroxene is modally abundant and occurs as large clusters (2–5 mm). The degree of recrystallization of the clusters varies, but is clearly lower than in type microstructure 2B. Scattering of orthopyroxene grains is moderate and pull-apart is common. An intricate intergrowth of smaller grains of orthopyroxene with spinel is typical.

Clinopyroxene occurs most commonly as interstitial grains to olivine (see fig. 3c in Suhr & Robinson 1993), variably associated with spinel and rarely with small amounts of orthopyroxene. In thin section, spatially separated grains of clinopyroxene may show simultaneous optical extinction, suggesting that the grains are connected in three dimensions (Fig. 5d). Simple diopside growth twins, a good indicator for direct precipitation from a melt (Raleigh & Talbot 1967, Nicolas & Poirier 1976), have been observed. The derivation of these clinopyroxene grains from trapped melt appears well substantiated. Clinopyroxene occurs also as small (0.3 mm) to large grains within the orthopyroxene clusters and rarely as isolated, larger grains. Spinel occurs invariably as small (0.1–0.4 mm), vermicular grains, mostly intergrown with clinopyroxene and/or orthopyroxene.

In order to evaluate the strain magnitude in TM 1181, the sample is compared to the high strain asthenospheric microstructure of unit 2. Within unit 5, the strength of the mineral-defined foliation and lineation is weak (vs moderate to strong in unit 2), lattice fabrics are only moderately strong (vs strong in unit 2), spinels are closely associated with pyroxenes (not the case in unit 2), the pyroxenes are pulled apart but poorly recrystallized (vs highly recrystallized and scattered in unit 2). In the field, pyroxenitic lithological banding in unit 5 tends to be sharply defined and is boudinaged or buckled, whereas it is very diffuse in unit 2. All features are compatible with lower strains at the base of unit 5 than at the top of unit 2.

Further up-section within unit 5, the microstructures become finer grained, less orthopyroxene-rich, and a

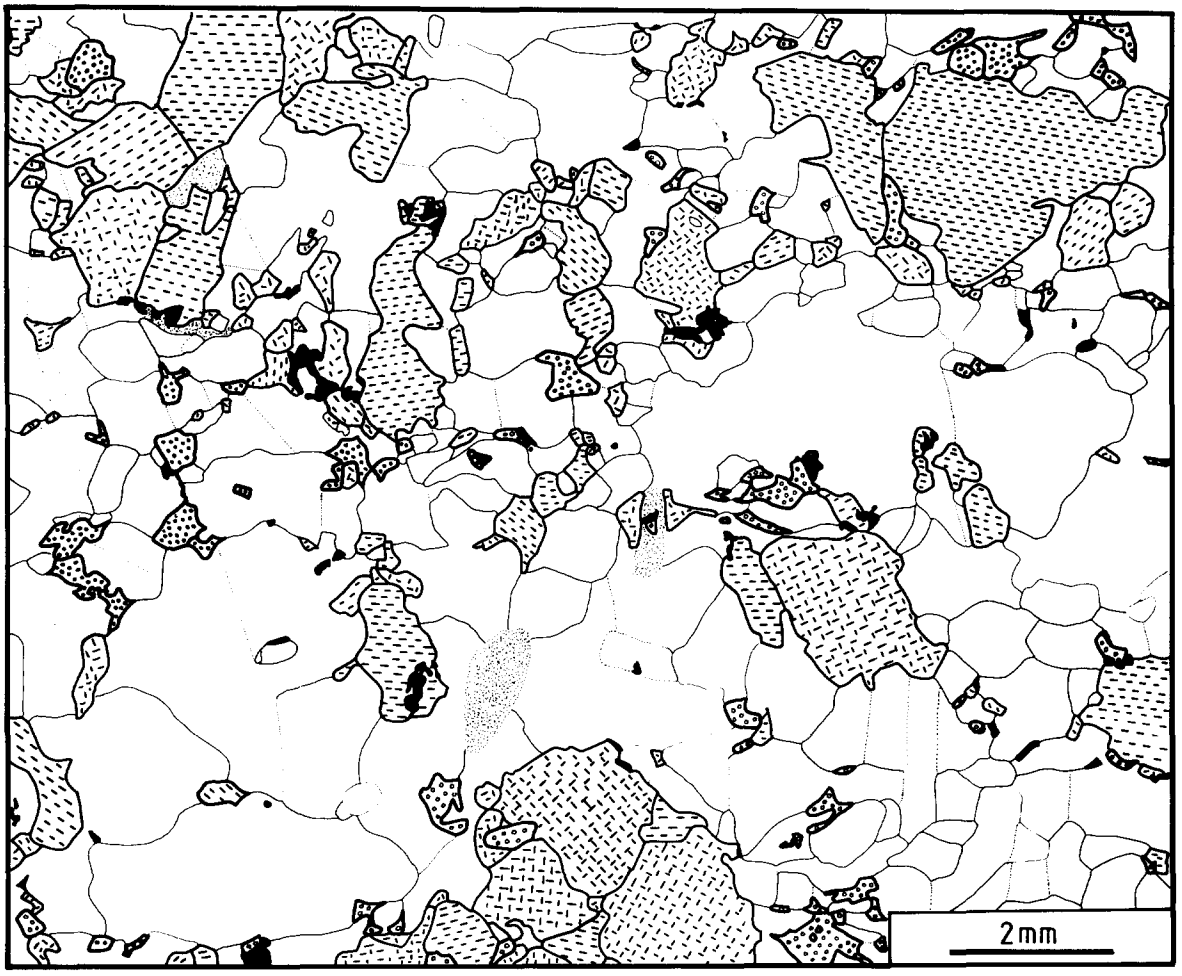

Fig. 12. Line drawing of type microstructure 5 (TM 1181), representing a low strain, high temperature harzburgite. For legend see Fig. 3.

lower temperature overprint is more pronounced, i.e. microstructures are similar to those of unit 3.

Type microstructure 6: *mylonitic, coarse-grained lherzolite*

The peridotites of unit 6 are all affected by a variably strong, lower temperature overprint. The type microstructure (TM 1056) represents a sample taken from a very high strain zone in the southeastern part of the massif. Such high strain zones stand out because the coarse orthopyroxene grains typical for the basal peridotites are extremely flattened.

The olivine microstructure is tabular equigranular (aspect ratio 3:1) and has a 100 × 30 μm average neoblast size (Fig. 6d), indicating σ_d = 60 MPa (for 65 μm). The neoblast grain size changes in layers and lenses parallel to the foliation, indicating partitioning of strain into certain layers. Adjacent to orthopyroxene porphyroclasts, the olivine grain size can be as low as 30 × 10 μm, indicating stress concentration next to orthopyroxenes. The abundance of olivine porphyroclasts is low, and they show abundant tilt walls. The maximum size of olivine porphyroclasts is 1 mm and their aspect ratio is<5. As orthopyroxene and clinopyroxene neoblasts cannot be distinguished with certainty from olivine neoblasts in the fine-grained matrix, petrofabric data were collected from a sample with a slightly coarser neoblast size, reflecting a less intense lower temperature overprint. Again, the activated slip system was (0*kl*)[100] (Fig. 8e).

Three types of orthopyroxene grains can be distinguished (Fig. 13). These are as follows.

(i) *Ribbon grains*. They have an average aspect of 10:1 but may reach 100:1. Within the ribbon grains, the traces of clinopyroxene exsolution lamellae and the orthopyroxene cleavage are invariably subparallel to the elongation of the grains and the foliation. As exsolution of high Ca-pyroxenes from enstatite occurs along the (100) plane of enstatite (e.g. Deer *et al.* 1966), activation of the well documented slip system (100)[001] of orthopyroxene is suggested.

(ii) *Porphyroclasts with low aspect ratios*. They have rounded outlines and apparently were microstructurally stiff, as orthopyroxene ribbon grains are bent around them. As indicated by the two visible, perpendicular cleavage traces in thin section, these grains are in an unfavourable orientation for slip and have consequently 'locked up' during deformation (Etchecopar 1977, Etchecopar & Vasseur 1987).

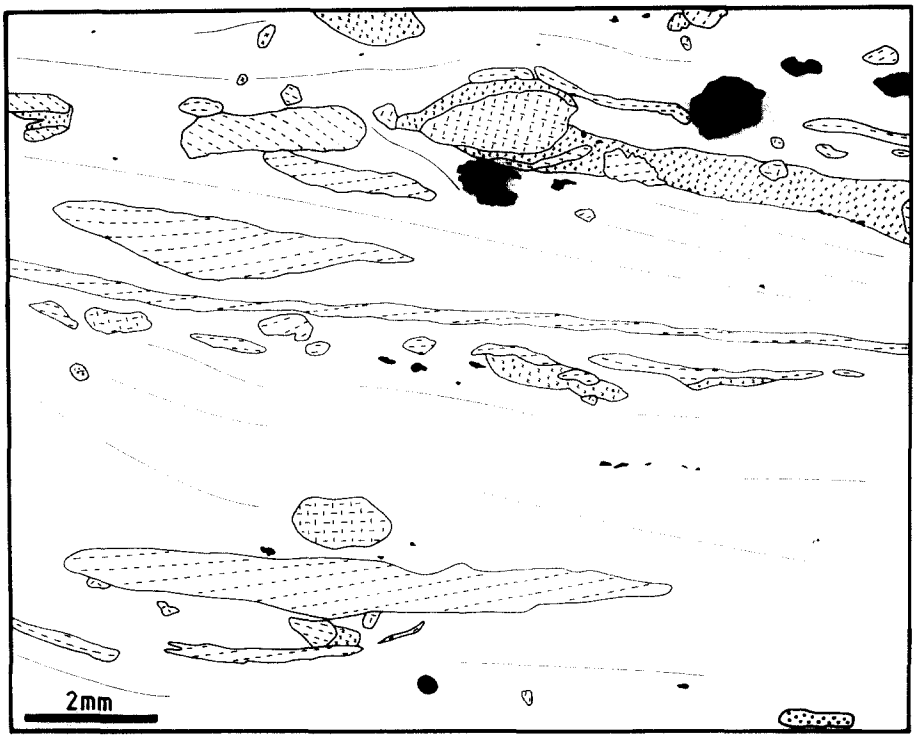

Fig. 13. Line drawing of type microstructure 6 (TM 1056), representing a mylonitic peridotite with coarse orthopyroxene grains; z-pattern—highly recrystallized orthopyroxene; continuous lines—foliation trend of olivine matrix. For further legend see Fig. 3.

(iii) *Orthopyroxene neoblasts*. They are in the 50 μm-range and are abundant as tails to 'hard' orthopyroxene porphyroclasts. They derive from (ii) by progressive recrystallization of the margins of porphyroclasts. They tend to be associated with vermicular spinel grains. Neoblasts also occur as scattered grains in the matrix.

Clinopyroxene occurs as rare porphyroclasts (up to 0.5 mm). It is probably abundant as a matrix mineral, but is difficult to distinguish from olivine. Spinel is present as tiny (20 μm), wormy grains in the olivine–orthopyroxene matrix. It is absent in unrecrystallized orthopyroxene porphyroclasts. In addition, spinel occurs as large grains (up to 1 mm, in other samples up to 3 mm) which may partly or totally enclose olivine and orthopyroxene. Several of the large grains are sometimes aligned in foliation-parallel layers.

Further microstructural features of unit 6

Within unit 6, the low strain peridotites of unit 5 are progressively deformed into protomylonitic and then mylonitic peridotites. A very similar microstructural sequence was illustrated by Boudier (1978) for peridotites from the Lanzo massif. Characteristic is the progressively increasing proportion of olivine neoblasts.

Within all samples studied from unit 6, the mean neoblast size of olivine varies normally between 150 μm for the lowest strain samples (i.e. the samples with the weakest mineral shape fabric) and 20 μm for the highest samples. In specific layers of the highest strain samples, the neoblast size may be as low as 2 × 5 μm. Even the fine-grained neoblasts are elongated and the lattice fabric is very strong (gypsum plate test), so that superplastic flow as significant deformation mechanism can be excluded. Stress values derived for the 150—20 μm neoblasts range from 20 to 165 MPa. Particularly in the lower and intermediate strain samples, a coarser and a finer grained neoblast generation or a whole range of neoblast generations usually are present within one sample (cf. Nicolas 1978). An average neoblast size is therefore difficult to determine. A best estimate for the intermediate strain samples is 90 μm (corresponding to 46 MPa). In intermediate strain samples, oblique olivine shape fabrics are developed (see under unit 4).

Within the same sequence of increasing strain, orthopyroxenes grade from large, uncrystallized grains or aggregates of grains into the three types described for the type microstructure. In the intermediate strain facies, orthopyroxene grains may be sliced up by trails of orthopyroxene neoblasts. In the highest strain microstructures, all but a few small, roundish porphyroclasts have disappeared. The shard-type orthopyroxene typical for unit 4 is not well developed.

Near the contact to the metamorphic sole, synkinematic, colourless amphibole occurs within cm-wide, and in one case up to 1 m wide, shear zones. Judging from the relative modal abundances in the shear zones and the host rocks, it is inferred that clinopyroxene first, and then orthopyroxene have progressively broken down. In extreme cases, the samples consist of a regular amphibole–olivine banding and pyroxenes are absent. Ultramafic ultramylonites occur within 1–3 m of the amphibolites of the metamorphic sole. The average grain size is rather even for all phases present, but varies from sample to sample between 20 and 100 μm. Amphibole is present in most of the ultramylonites in bands

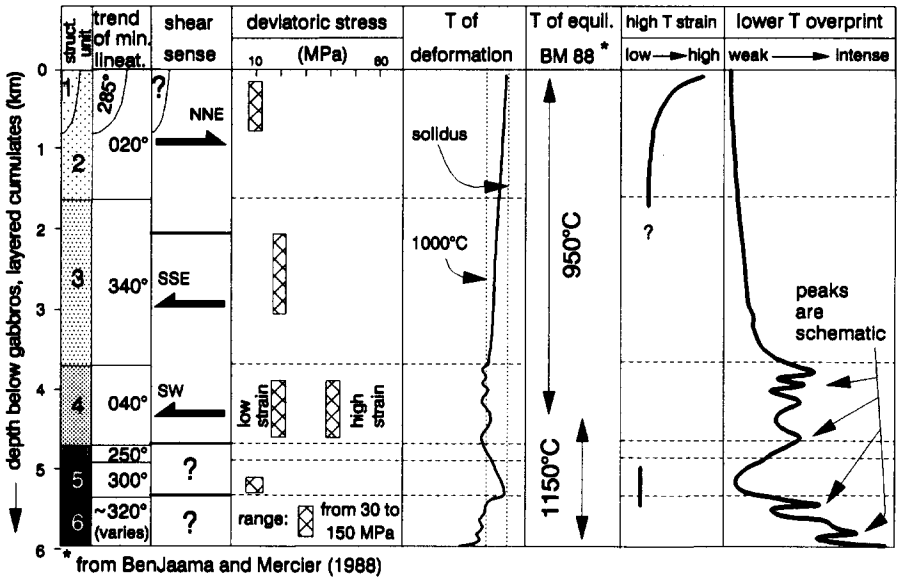

Fig. 14. Compilation of important field and microstructural characteristics in the Table Mountain peridotite section.

replacing clinopyroxene. Spinel tends to be brown–red, but green spinel occurs locally and may alternate within a single thin section in bands with red spinel. In the immediate contact area between peridotite with the metamorphic sole, interbanding of amphibolite–granulite with peridotite is observed. This interbanding is present even on the thin section scale. The ultramylonites are considered metasomatized peridotites (Church 1972, Malpas 1979, McCaig 1981). An olivine lattice fabric analysis was performed for one of the coarser grained ultramylonite specimens (Fig. 8f). The pattern is difficult to interpret. The activation of several different slip systems is suggested. Olivine lattice fabrics are typically weaker for basal ophiolitic peridotites deformed at lower temperatures (Nicolas *et al.* 1980, Boudier *et al.* 1988).

DISCUSSION

One of the remarkable features of the TM mantle section is the range of different microstructures preserved. High temperature, spreading-related microstructures appear in peridotites with high strains (type 2B) and relatively low strains (type 5). Estimating strain magnitudes is difficult in the high temperature dunites (type 2A) where only elongated spinels and strong olivine lattice fabrics indicate the deformed state. The weak disintegration of orthopyroxene–spinel clusters suggests that the total strain within unit 3 was lower than within unit 2. Melt impregnation is most common in the uppermost peridotites (types 1 and 2B). A weak, fairly homogeneous, lower temperature overprint is typical for unit 3 (type 3) whereas a strong, but heterogeneous lower temperature overprint is characteristic for unit 4 (type 4). Lower temperature, detachment-related strain is preserved in unit 6, culminating in orthopyroxene ribbon mylonites (type 6) and ultramafic ultramylonites adjacent to the metamorphic sole. The most important variables in the TM mantle section are summarized in Fig. 14. A model suggesting tectonic regimes for the different structural units and the microstructural variation in the TM mantle section was presented in Suhr (1992).

Melt-infiltration

Geochemical and field evidence suggests that the typically clinopyroxene-rich, uppermost peridotites in TM have not undergone a lower degree of partial melting than the underlying, clinopyroxene-poor harzburgites; rather they have undergone chemical re-enrichment by infiltrating melts (Suhr & Robinson 1993). Most melt-related clinopyroxene occurs interstitially in the olivine grain boundary network and is not associated with orthopyroxene grains. Such a spatial arrangement is consistent with the surface equilibrium morphology of basaltic melt in peridotite during hydrostatic conditions (Waff & Balau 1979, Fujii *et al.* 1986, Toramaru & Fujii 1986). The incomplete extraction of the melt observed in the uppermost peridotites is a well-known problem which was addressed by Rabinowicz *et al.* (1987) and Nicolas (1990). Another remarkable feature is the enrichment of clinopyroxene grains in bands parallel to the foliation (or flow plane?). It argues strongly in favour of the syntectonic nature of the impregnations (Nicolas & Jackson 1982).

Temperatures of deformation

The term 'very high temperature' microstructure is used here to denote a low stress, well-recovered olivine microstructure, typically with evidence for hypersolidus flow in the form of undeformed to weakly deformed melt impregnation textures within a deformed olivine matrix. Inferred temperatures of deformation are near the solidus of depleted upper mantle under the low

pressure conditions preserved in ophiolites, i.e. 1200–1250°C (Jaques & Green 1980, Takahashi & Kushiro 1983). Such high temperatures of deformation are also required by models which simulate the heat required to generate the oceanic crustal thickness present in the Bay of Islands ophiolite (5–7 km) by decompression melting of peridotite (McKenzie 1984). An estimate of 1300°C is given for the asthenospheric microstructures by Nicolas (1986a).

The peridotites of unit 6 and the microstructurally similar high strain zones of unit 4 are equivalent to the 'lithospheric' microstructures of Nicolas (1986a). His estimate for the deformation temperatures for these microstructures is 900–1000°C, a value that should apply to the bulk of unit 6. The basal ultramylonites show diffuse olivine lattice fabrics different from those of the rest of unit 6, so a value <900°C should apply to them.

It is difficult to estimate a temperature of deformation for microstructures with a weak, lower temperature overprint (unit 3, lower strain part of unit 4, top of unit 5). It is possible that unit 3 could simply reflect small, lower temperature strains acquired during deformation in the same temperature regime as that of unit 6. Compared to unit 6 and high strain zones of unit 4, the microstructures of unit 3 are marked by the absence of: (i) moderately elongated olivine grains, (ii) oblique olivine shape fabrics; and (iii) clear strain partitioning in the field. All three features of unit 6 and high strain rocks of unit 4 are also absent in the very high temperature peridotites, and they may be related to strain-induced rheological hardening associated with decreasing temperatures of deformation. In addition, the neoblast size is smaller in the strongly lithospheric microstructures. Therefore the temperatures of deformation of unit 3 are considered higher than those of unit 6, i.e. between 1000 and 1100°C.

Equilibration temperatures for the TM mantle section were determined by Ben Jamaa & Mercier (1988). Their calculations (based on a 7 km thick mantle section) showed that the upper 5 km of the mantle section equilibrated at 950°C and the basal 2 km at 1150°C. Therefore, for large parts of the mantle section, the temperatures of deformation do not correlate well with the temperatures of equilibration. The only obvious correlation to the equilibration temperatures is found in the grain size of orthopyroxene. Coarse-grained peridotites occur in the basal mantle section and finer grained peridotites in the upper section. It is therefore possible that the high temperatures of equilibration are preserved due to the increased memory capacity present in the cores of large orthopyroxene grains within units 5 and 6. However, Suhr (1992) has suggested that along the boundary of units 4 and 5, two mantle sequences are juxtaposed which have experienced a different flow and therefore also cooling history. As the cooling rate is a primary factor in determining equilibration temperatures in peridotites (Nicolas 1986a), the different PT estimates for basal peridotites may, in accordance with Ben Jamaa & Mercier (1988), be more than only a grain size effect.

Olivine slip systems

Several studies suggested that, depending on the temperature of deformation, different olivine slip systems are activated (Carter & Avé Lallement 1970, Goetze 1978, Nicolas *et al.* 1980, Nicolas & Christensen 1987). At high and very high (hypersolidus) temperatures ($T >$ 1100°C), the olivine slip system (010)[100] is dominant; under moderate and low temperatures (700–1000°C), the pencil glide system (0*kl*)[100] is activated. At low temperatures, the additional activation of the system (010)[001] (Nicolas & Christensen 1987) or (110)[001] (Carter & Avé Lallement 1970) was proposed. According to Nicolas & Christensen (1987), activation of the system (001)[100] is characteristic for very high temperatures of deformation. This slip system has been reported for example, by Smewing *et al.* (1984) from the Oman ophiolite, but also by Mercier (1985) and Girardeau & Mercier (1988) from lithospheric, lower temperature peridotites.

In the TM samples, a small but consistent asymmetry between foliation and the olivine lattice fabric suggests that a significant component of rotational strain was present (e.g. Bouchez *et al.* 1983). This obliquity allows one to determine the shear sense. Recent criticism concerning this method to determine the sense of shear (Takeshita *et al.* 1990) is not justified because in the simulations by Takeshita *et al.* (1990) and Ribe & Yu (1991), the shape fabric was not determined and the relative orientation of the lattice fabric with respect to the foliation is consequently unknown. The lattice data from TM show that the slip direction always coincides with $[100]_{\text{olivine}}$. There appears to be a slight preference for the activation at higher temperatures of slip planes with low indices ((010), (001), (011)). At lower temperatures, the entire range of (0*kl*) planes are common as slip planes (a total of 14 samples considered in Suhr 1991). Because the preference for the low indices is rather weak, information about the temperatures of deformation from olivine petrofabrics should only be obtained from a suite of samples as opposed to single samples. An exceptional olivine lattice fabric is present in the basal ultramylonite. It represents the simultaneous activation of several slip systems.

Strain rate estimates

Given the deviatoric stress and temperature of deformation for an olivine dominated peridotite, strain rates can be estimated with available dunite flow laws. A number of olivine and dunite flow law data are plotted in Fig. 15(a). Fortunately, for dry, subsolidus dunites, the discrepancies between the more recent flow laws shown in Fig. 15(a) result only in a variation of the strain rates by about one order of magnitude. However, application of the flow law of Post (1977) would yield strain rates which are about two orders of magnitude lower than the ones of Fig. 15(a). For wet dunites, the discrepancies are higher (Fig. 15a). For an average detachment microstructure of unit 6 (950°C and 46 MPa), the flow law of

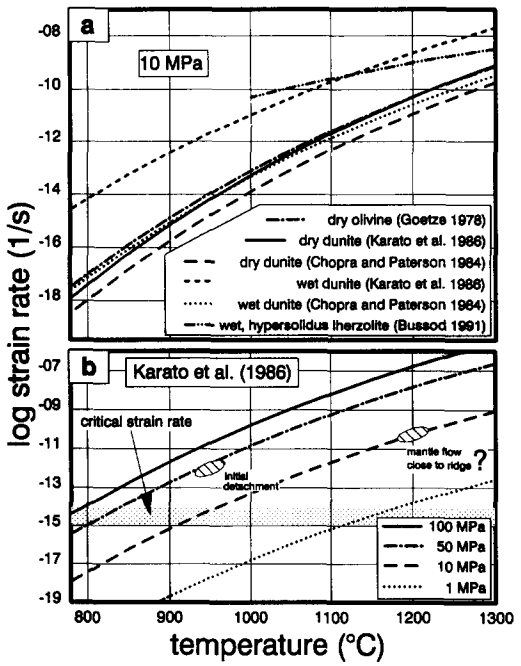

Fig. 15. (a) Temperature–strain rate relationships for dry and wet dunite and hypersolidus lherzolite at 10 MPa deviatoric stress. (b) Same as in (a) but showing the flow law of Karato *et al.* (1986) for different levels of stress. Shaded area marks the 'critical strain rate' below which deformation is geologically irrelevant. Ruled fields are conditions constrained by microstructural parameters in Table Mountain. For discussion, see text.

Karato *et al.* (1986) yields a strain rate of 1.4×10^{-12} s^{-1} (Fig. 15b).

This strain rate can be evaluated in a simplified tectonic scenario: it is assumed that detachment occurred by converging plates having oppositely directed velocities of 3 cm year^{-1} each. The relative velocity along the detachment plane was therefore 6 cm year^{-1}. Unit 6, which is related to detachment, has an average width of 500 m. A similar thickness (300–500 m) for the basal detachment fabrics has been observed in the Lewis Hills and Blow Me Down Mountain (Suhr & Cawood in press). Unit 6 may represent the half-width of the shear zone along which detachment took place by simple shear. The other half of the shear zone, the footwall during ophiolite obduction, was left behind during continued thrusting. In a further simplification it is assumed that the strain distribution across the 1000 m wide shear zone was homogeneous. The shear strain rate $\dot{\gamma}$ can then be calculated as the ratio of the displacement across the entire width of the shear zone per time interval to the shear zone width. For instantaneous conditions, $\dot{\gamma}$ is related to the principle strain rates ($\dot{e}_1$, $\dot{e}_3$) by $\dot{\gamma} = 2\dot{e}_1 = -2\dot{e}_3$ (Ramsay 1980). An $\dot{e}_1$ value of 9.5×10^{-13} s^{-1} is obtained.

A strain rate estimate can also be made for the asthenospheric microstructure using 1200°C and 10 MPa (neoblast size 550 μm). Using the flow laws of Karato *et al.* (1986) and Chopra & Paterson (1984), the very high strain rates of 5.4×10^{-11} and 1.2×10^{-11} s^{-1}, respectively, are obtained. Alternatively, the uppermost peridotites of unit 2 may represent frozen in hypersolidus flow structures with a temperature of deformation of 1250°C. In this case the piezometer of Bussod & Christie (1991) and the flow law of Bussod (1991), both calibrated during (hydrous) hypersolidus conditions, can be applied. For an average neoblast size of 550 μm, only 2.2 MPa are indicated. This low deviatoric stress results, however, in a strain rate of 1.3×10^{-11} s^{-1} because in the presence of melt some (Cooper & Kohlsted 1986) or very significant (Green & Borch 1990, Bussod 1991) rheological weakening of peridotite occurs. The weakening of several orders of magnitude occurs even though dislocation glide remains the rate limiting factor (Green & Borch 1990, Bussod & Christie 1991).

Numerical modelling for deformation of peridotites in a melt charged, *forced* flow regime yields strain rates of 10^{-12} s^{-1} (Ceuleneer *et al.* 1988). However, for peridotites of unit 2, a *plate driven* mantle flow was inferred (Suhr 1992). In such a setting, the zone of active deformation between the overlying rigid lithosphere and the underlying asthenosphere would have to be extremely thin (in the order of 20–100 m) in order to produce strain rates of 1×10^{-11}–5×10^{-11} s^{-1}. The only realistic way to produce a narrow high strain zone would be the abundant presence of melt which may then lead to decoupling between the asthenosphere and lithosphere (Rabinowicz *et al.* 1987).

In summary, estimates for strain rates during detachment and very high temperature spreading are both higher than typical geological strain rates, the latter being between 10^{-13} and 10^{-15} s^{-1} (Pfiffner & Ramsay 1982, Carter & Tsenn 1987). Higher strain rates may, however, be reached in mylonite zones and both areas are considered zones of strain concentration. For the case of initial detachment, the microstructurally derived strain rate, in combination with the flow law of Karato *et al.* (1986), is in good agreement with a simplified plate tectonic scenario. The predicted strain rates for the very high temperature, low stress peridotites appear to be at the very high end of realistic scenarios. This applies in particular to peridotites of unit 5 where it was inferred that accumulated strain is only moderate to low. Some potential causes for excessively high strain rate estimates are: (i) inhibited growth of neoblasts during natural deformation compared to the experimental runs (see also below); (ii) overestimate of temperature of deformation for the olivine matrix; for example, an error of 50°C in the temperature estimate results in a strain rate which varies by nearly one order of magnitude; and (iii) the applied olivine rheology (flow law) is too weak; large errors in the flow law may occur during extrapolation from laboratory to natural conditions. For example, the discrepancy for the flow laws of wet dunite (Fig. 15a) is much lower during laboratory conditions than after extrapolation to natural conditions; and (iv) inaccurate piezometer.

Preservation of microstructures

During static annealing microstructures tend to coarsen, driven by the energy stored in dislocations and grain boundaries. Grain growth rates increase with high tem-

peratures. Using the square grain growth law for dry olivine given in Karato (1989), a grain size typical for the detachment fabrics (90 μm at 950°C) would be reached within half a year by static annealing alone. [A value of 5×10^{-7} m^2 s^{-1} was adopted for the constant k_0 to match the growth relation given in fig. 14 of Karato (1989). A perfect match was not obtained. In general, under dry conditions, the growth conditions are not yet well constrained (Karato written communication 1992)]. The 10-fold grain size is reached in 50 years. The presence of water would accelerate grain growth. Grain growth is more effective for small grains than for large grains (Twiss 1977, Tullis & Yund 1982) so that it could be expected that the preservation of large grain sizes in very high temperature microstructures is less of a problem than the freezing of small grains in the detachment fabrics. However, as the inferred temperatures are higher for the very high temperature peridotites, annealing under these temperatures would also be rapid: a grain size of 550 μm would be reached (at 1200°C) within 0.5 years, and the 10-fold grain size within 54 years. The geologically small time spans needed for growth of olivine suggest that grain growth in the peridotites from TM was impeded. This is supported by the occurrence of thin (<1 mm), entirely recrystallized olivine bands in peridotites of unit 6 with an average grain size of only 2×5 μm. At 900°C (850°C), such small olivine grains should only exist for 14 (40) h. Evidence for grain growth of olivine was safely recognized only within dunites of the type microstructures 1 and 2A. Growth in the peridotites, with the exception of some dunites, must therefore have been highly hindered by impurities (secondary phases or pores) (Karato 1989). While harzburgite and lherzolite microstructures from TM are considered primary mantle microstructures, the implied relative stability of the olivine grain boundaries is still poorly understood.

Lithosphere–asthenosphere boundary and origin of lithospheric microstructures

Peridotite microstructures together with olivine flow laws can be used to evaluate the location of the lithosphere–asthenosphere boundary (e.g. Tapponnier & Francheteau 1978). The asthenosphere should be characterized by the ability to undergo a significant amount of deformation when low stresses (<10 MPa; Goetze *et al.* 1978, Nicolas 1978) are applied. Strain rates $>10^{-15}$ s^{-1} are considered significant over geological time scales (e.g. Pfiffner & Ramsay 1982). Using the flow laws of Karato *et al.* (1986) and Chopra & Paterson (1984), a strain rate of 10^{-15} s^{-1} can be reached during a 10 MPa deviatoric stress at >900–950°C, respectively (Fig. 15a). Consequently, the rheological asthenosphere may coincide with an isotherm as low as 900°C and thus be clearly subsolidus. Microstructural characteristics of peridotites deformed at 900 or 1000°C are such that they are classified as 'lithospheric' (Nicolas 1986a, Ceuleneer *et al.* 1988). The flow law data indicate that they *could*, however, form within the rheological asthenosphere. The final answer whether such lower temperature microstructures in peridotites may also be correlated with the spreading history (Girardeau & Mercier 1988) must therefore come from the regional geological context.

For example, along the entire base of the Bay of Islands ophiolite, the basal peridotites show a strong lower temperature overprint which is dying out upsection and is geometrically identical to the underlying amphibolites of the metamorphic sole. Obviously, the structures within these peridotites formed during ophiolite detachment. In TM, the tectonic origin of the moderately lithospheric unit 4 is debatable (Suhr 1992). It is geometrically distinct from peridotites in the hanging- and footwall, but distinct microstructures are restricted to high strain zones. The geometrical change was used to favour a formation during the earliest detachment history. In the Oman ophiolite, zones of lower temperature peridotites within the mantle section are arranged as steep shear zones which can be traced into the basal, detachment-related peridotites and the metamorphic sole (Boudier *et al.* 1988, Ceuleneer *et al.* 1988). Again, a detachment origin is indicated for the lower temperature microstructures though they occur at significant distance to the metamorphic sole. In the dunite–harzburgite transition of the eastern Lewis Hills (Fig. 1), high and lower temperature microstructures are interleaved and show the same orientations of foliations and mineral stretching lineations (Suhr & Cawood unpublished data). In this case, a spreading-related origin of the lithospheric microstructures could be indicated. Apparently, migration and freezing of the flow was not as effective in the Lewis Hills as in TM. In the southern Lewis Hills, a major, more than 100 m thick, lower temperature shear zone is located near the crust–mantle interface (Dunsworth *et al.* 1986) and can be traced across the entire eastern Lewis Hills (Suhr & Cawood unpublished). There are indications that the geometry is extensional and the shear zone may be related to reactivation of the lithosphere during the abundant late magmatism in the Lewis Hills.

In a more general sense, four tectonic situations appear most relevant when looking for the generation of higher stress, lower temperature upper mantle peridotites during the spreading phase of ophiolitic rocks.

(i) during generation of ophiolites in which the emergence temperature of the upper mantle is relatively cold (e.g. McKenzie 1984, Nicolas 1986b). An example would be the slow spreading Xigaze ophiolite (Girardeau & Mercier 1988);

(ii) in the dying stages of spreading-related flow, i.e. the final stages of conversion of ductile asthenospheric mantle into rigid oceanic lithosphere as the plates move away from the spreading centre. An example would be the weak, lower temperature overprint observed in unit 3 of TM;

(iii) during shear of mantle rocks along a 'cold wall', e.g. next to transform faults. The application of the microstructural characteristics and inferred deformation conditions from TM to this regime is, however, dangerous, as hydrous deformation is more likely to occur next

to transform faults. In the presence of water, olivine microstructures (e.g. Nicolas 1986a) and rheological parameters (Fig. 15) are distinctly different;

(iv) during reactivation of rigid, colder oceanic lithosphere, e.g. at ridge–transform intersections, propagating rifts, and during off-axis diapirism.

Whether for a given occurrence of lower temperature, high stress mantle peridotites in an ophiolite one of these scenarios applies or whether true detachment tectonics must be invoked should be carefully evaluated. The relative abundance of high temperature vs lower temperature microstructures within a peridotite sequence, combined with regional field evidence, may then provide important constraints about the flow and cooling dynamics beneath an oceanic spreading centre.

Acknowledgements—The author benefitted from discussions with Tom Calon, Peter Cawood, Sherry Dunsworth, Jeroen van Gool, and a visit at the Laboratoire de Tectonophysique (USTL Montpellier, France) run by Adolphe Nicolas. Constructive reviews by Jeffrey Karson, Shun Karato, and Joseph White and careful handling by Steven Wojtal are gratefully acknowledged and improved the manuscript. Parks Canada is thanked for permitting field work and sampling in the Gros Morne National Park. The author also wants to take the opportunity to thank faculty, staff, and students of the Department of Earth Sciences for an exciting and educational time in Newfoundland. Funding for the study was provided by a Memorial University of Newfoundland graduate fellowship.

REFERENCES

Ben Jamaa, N. & Mercier, J.-C. C. 1988. Major elements phase chemistry of ophiolitic harzburgites from western Newfoundland. *Terra Cognita* **7**, 355.

Bouchez, J.-L., Lister, G. S. & Nicolas, A. 1983. Fabric asymmetry and shear sense in movement zones. *Geol. Rdsch.* **72**, 401–419.

Boudier, F. 1978. Structure and petrology of the Lanzo peridotite massif (Piedmont Alps). *Bull. geol. Soc. Am.* **89**, 1574–1591.

Boudier, F., Ceuleneer, G. & Nicolas, A. 1988. Shear zones, thrusts and related magmatism in the Oman ophiolite: initiation of thrusting on an oceanic ridge. *Tectonophysics* **151**, 275–296.

Boullier, A. M. & Gueguen, Y. 1975. SP-mylonites: origin of some mylonites by superplastic flow. *Contr. Miner. Petrol.* **50**, 93–104.

Boullier, A. M. & Nicolas, A. 1975. Classification of textures and fabrics of peridotite xenoliths from South African kimberlites. *Phys. Chem. Earth* **9**, 467–475.

Bussod, G. Y. 1991. The rheology of a partially molten upper mantle: laboratory and field measurement constraints. *Eos* **72**, 508.

Bussod, G. Y. & Christie, J. M. 1991. Textural development and melt topology in spinel lherzolite experimentally deformed at hypersolidus conditions. In: *Orogenic Lherzolites and Mantle Processes* (edited by Menzies, M. A., Dupuy, C. & Nicolas, A.). Oxford University Press, Oxford, 17–40.

Cannat, M., Bideau, D. & Hébert, R. 1990. Plastic deformation and magmatic impregnation in serpentinized ultramafic rocks from the Garret transform fault. *Earth Planet. Sci. Lett.* **101**, 216–232.

Carter, N. L. 1976. Steady state flow of rocks. *Rev. Geophys. & Space Phys.* **14**, 301–360.

Carter, N. L. & Avé Lallement, H. G. 1970. High temperature flow of dunite and peridotite. *Bull. geol. Soc. Am.* **81**, 2181–2202.

Carter, N. L. & Tsenn, M. C. 1987. Flow properties of continental lithosphere. *Tectonophysics* **136**, 27–63.

Ceuleneer, G., Nicolas, A. & Boudier, F. 1988. Mantle flow patterns at an oceanic spreading centre: the Oman peridotites record. *Tectonophysics* **151**, 1–26.

Chopra, P. N. & Paterson, M. S. 1984. The role of water in the deformation of dunite. *J. geophys. Res.* **78**, 7861–7876.

Church, W. R. 1972. Ophiolite: its definition, origin as oceanic crust, and mode of emplacement in orogenic belts, with special reference to the Appalachians. In: *The Ancient Oceanic Lithosphere* (edited by Irving, E.). Dept of Energy, Mines and Resources Canada, Ottawa, 71–85.

Church, W. R. & Riccio, L. 1977. Fractionation trends in the Bay of Islands ophiolite of Newfoundland: polycyclic cumulate sequence in ophiolites and their classification. *Can. J. Earth Sci.* **14**, 1156–1165.

Cooper, R. F. & Kohlstedt, D. L. 1986. Rheology and structure of olivine-basalt partial melts. *J. geophys. Res.* **91**, 9315–9323.

Darot, M. & Boudier, F. 1975. Mineral lineations in deformed peridotites: kinematic meaning. *Pétrologie* **1**, 225–236.

Deer, W. A., Howie, R. A. & Zussman, J. 1966. *An Introduction to the Rock Forming Minerals*. Longman, Harlow.

Drury, M. R., Hoogerduijn Strating, E. H. & Vissers, R. L. M. 1990. Shear zone structures and microstructures in mantle peridotites from the Voltri massif, Ligurian Alps, N. W. Italy. *Geologie Mijnb.* **69**, 3–17.

Dunsworth, S., Calon, T. & Malpas, J. 1986. Structural and magmatic controls on the internal geometry of the plutonic complex and its chromite occurrences in the Bay of Islands ophiolite, Newfoundland. *Geol. Surv. Can.* **86-1B**, 471–482.

Etchecopar, A. 1977. A plane kinematic model of progressive deformation in a polycrystalline aggregate. *Tectonophysics* **39**, 121–139.

Etchecopar, A. & Vasseur, G. 1987. A 3-D kinematic model of fabric development in polycrystalline aggregates: comparisons with experimental and natural examples. *J. Struct. Geol.* **9**, 705–717.

Etheridge, M. A. 1975. Deformation and recrystallisation of orthopyroxene from the Giles complex, central Australia. *Tectonophysics* **25**, 87–114.

Evans, C. & Hawkins, J. W. 1989. Compositional heterogeneities in upper mantle peridotites from the Zambales Range Ophiolite, Luzon, Philippines. *Tectonophysics* **168**, 23–41.

Fujii, N., Osamura, K. & Takahashi, E. 1986. Effect of water saturation on the distribution of partial melt in the olivine-plagioclase system. *J. geophys. Res.* **91**, 9253–9259.

Girardeau, J. & Mercier, J.-C. C. 1988. Petrology and texture of the ultramafic rocks of the Xigaze ophiolite (Tibet): constraints for mantle structure beneath slow-spreading ridges. *Tectonophysics* **147**, 33–58.

Girardeau, J. & Nicolas, A. 1981. The structures of two ophiolite massifs, Bay of Islands, Newfoundland: a model for the oceanic crust and upper mantle. *Tectonophysics* **77**, 1–34.

Goetze, C. 1978. The mechanisms of creep in olivine. *Phil. Trans. R. Soc. Lond.* **A288**, 99–109.

Green, H. W. II, & Borch, R. S. 1990. The rheology and microstructure of partially molten lherzolite experimentally deformed under upper mantle pressures and temperatures. *Terra Abstracts* **2**, 24.

Harte, B. 1977. Rock nomenclature with particular relation to deformation and recrystallisation textures in olivine-bearing xenoliths. *J. Geol.* **85**, 279–288.

Himmelberg, G. R. & Loney, R. A. 1980. Petrology of ultramafic and gabbroic rocks of the Canyon Mountain ophiolite, Oregon. *Am. J. Sci.* **280-A**, 232–268.

Jaques, A. L. & Green, D. H. 1980. Anhydrous melting of peridotite at 0–15 Kb pressure and the genesis of tholeiitic basalts. *Contr. Miner. Petrol.* **73**, 287–310.

Karato, S. 1984. Grain-size distribution and rheology of the upper mantle. *Tectonophysics* **104**, 155–176.

Karato, S. 1989. Grain growth kinetics in olivine aggregates. *Tectonophysics* **168**, 255–273.

Karato, S., Paterson, M. S. & FitzGerald, J. D. 1986. Rheology of synthetic olivine aggregates: influence of grain size and water. *J. geophys. Res.* **91**, 8151–8176.

Karato, S., Toriumi, M. & Fujii, T. 1980. Dynamic recrystallization of olivine single crystals during high-temperature creep. *Geophys. Res. Lett.* **7**, 649–652.

Karato, S., Toriumi, M. & Fujii, T. 1982. Dynamic recrystallization and high-temperature rheology of olivine. In: *High Pressure Research in Geophysics* (edited by Akimoto, S. & Manghnani, M. H.). *Adv. Earth Planet Sci.* **12**, 171–189.

Karson, J. & Dewey, J. F. 1978. Coastal Complex, western Newfoundland: an early Ordovician oceanic fracture zone. *Bull. geol. Soc. Am.* **89**, 1037–1049.

Malpas, J. 1978. Magma generation in the upper mantle, field evidence from ophiolite suites, and application to the generation of oceanic lithosphere. *Phil. Trans. R. Soc. Lond.* **A288**, 527–545.

Malpas, J. 1979. The dynamothermal aureole of the Bay of Islands ophiolite suite. *Can. J. Earth Sci.* **16**, 2086–2101.

McCaig, A. M. 1981. Metasomatic and isochemical metamorphic changes in the basal peridotite of the Bay of Islands Complex during ophiolite emplacement. *J. Struct. Geol.* **3**, 337.

McKenzie, D. 1984. The generation and compaction of partially molten rock. *J. Petrol.* **25**, 713–765.

Mercier, J.-C. C. 1985. Olivine and Pyroxenes. In: *Preferred Orientation in Deformed Metals and Rocks* (edited by Wenk, H.-R.). Academic Press, Orlando, 407–430.

Mercier, J.-C., Anderson, D. A. & Carter, N. L. 1977. Stress in the lithosphere: inferences from steady state flow of rocks. *Pure & Appl. Geophys.* **115**, 199–226.

Mercier, J.-C. & Nicolas, A. 1975. Textures and fabrics of upper mantle peridotites as illustrated by xenoliths from basalts. *J. Petrol.* **16**, 454–487.

Nazé, L., Doukhan, N., Doukhan, J. C. & Latrons, K. 1987. A TEM study of lattice defects in naturally and experimentally deformed orthopyroxenes. *Bull, Minéral.* **110**, 497–512.

Nicolas, A. 1978. Stress estimates from structural studies in some mantle peridotites. *Phil. Trans. R. Soc. Lond.* **A288**, 49–57.

Nicolas, A. 1986a. Structure and petrology of peridotites: clues to their geodynamic environment. *Rev. Geophys.* **24**, 875–895.

Nicolas, A. 1986b. A melt extraction model based on structural studies in mantle peridotites. *J. Petrol.* **27**, 999–1022.

Nicolas, A. 1990. Melt extraction from mantle peridotites: hydrofracturing and porous flow, with consequences for oceanic ridge activity. In: *Magma Transport and Storage* (edited by Ryan, M. P.). J. Wiley & Sons, Chichester, 159–173.

Nicolas, A., Boudier, F. & Bouchez, J.-L. 1980. Interpretation of peridotite structures from ophiolitic and oceanic environments. *Am. J. Sci.* **280-A**, 192–201.

Nicolas, A. & Christensen, N. I. 1987. Formation of anisotropy in upper mantle peridotites—a review. In: *Composition, Structure and Dynamics of the Lithosphere–Asthenosphere System* (edited by Fuchs, K. & Froidevaux, C.). *Am. Geophys. Un. Geodyn. Ser.* **16**, 111–123.

Nicolas, A. & Dupuy, C. 1984. Origin of ophiolitic and oceanic lherzolites. *Tectonophysics* **110**, 177–187.

Nicolas, A. & Jackson, M. 1982. High temperature dikes in peridotites: origin by hydraulic fracturing. *J. Petrol.* **23**, 568–582.

Nicolas, A. & Poirier, J. P. 1976. *Crystalline Plasticity and Solid State Flow in Metamorphic Rocks*. John Wiley & Sons, London.

Pfiffner, O. A. & Ramsay, J. G. 1982. Constraints on geological strain rates: arguments from finite strain states of naturally deformed rocks. *J. geophys. Res.* **87**, 311–321.

Pike, J. E. & Schwarzman, E. C. 1977. Classification of textures in ultramafic xenoliths. *J. Geol.* **85**, 49–61.

Post, R. L. 1977. High temperature creep of Mt. Burnet dunite. *Tectonophysics* **42**, 75–100.

Rabinowicz, M., Ceuleneer, G. & Nicolas, A. 1987. Melt segregation and flow in mantle diapirs below spreading centers: evidence from the Oman ophiolite. *J. geophys. Res.* **92**, 3475–3486.

Raleigh, C. B. & Talbot, J. L. 1967. Mechanical twinning in naturally and experimentally deformed diopside. *Am. J. Sci.* **265**, 151–165.

Ramsay, J. G. 1980. Shear zone geometry: a review. *J. Struct. Geol.* **2**, 83–99.

Ribe, N. M. & Yu, Y. 1991. A theory of plastic deformation and textural evolution of olivine polycrystals. *J. geophys. Res.* **96**, 8325–8335.

Ross, J. V., Avé Lallement, H. G. & Carter, N. L. 1980. Stress dependence of recrystallized-grain and subgrain size in olivine. *Tectonophysics* **70**, 39–61.

Smewing, J. D., Christensen, N. I., Bartholomew, I. D. & Browning, P. 1984. The structure of the oceanic upper mantle and lower crust as deduced from the northern section of the Oman ophiolite. In: *Ophiolites and Oceanic Lithosphere* (edited by Gass, I. G., Lippard, S. J. & Shelton, A. W.). *Spec. Publs geol. Soc. Lond.* **13**, 41–53.

Suhr, G. 1991. Structural and magmatic history of upper mantle peridotites in the Bay of Islands Complex, Newfoundland. Unpublished Ph.D. thesis, Memorial University, St. John's.

Suhr, G. 1992. Upper mantle peridotites in the Bay of Islands Ophiolite, Newfoundland: formation during the final stages of a spreading centre? *Tectonophysics* **206**, 31–53.

Suhr, G., Calon, T. & Dunsworth, S. M. 1991. Origin of complex upper mantle structures in the southern Lewis Hills (Bay of Islands Ophiolite, Newfoundland). *Can. J. Earth Sci.* **28**, 774–787.

Suhr, G. & Cawood, P. A. In press. Structural history of ophiolite obduction, Bay of Islands, Newfoundland. *Bull. geol. Soc. Am.*

Suhr, G. & Robinson, P. T. 1993. Origin of mineral chemical stratification in the mantle section of the Table Mountain Massif (Bay of Islands Ophiolite). *Lithos.* **105**, 399–410.

Takeshita, T., Wenk, H.-R., Canova, G. R., & Molinari, A. 1990. Simulation of dislocation-assisted plastic deformation in olivine polycrystals. In: *Deformation Processes in Minerals, Ceramics and Rocks* (edited by Barber, D. J. & Meredith, P. G.). Unwin Hyman, London, 365–376.

Tapponnier, P. & Francheteau, J. 1978. Necking of the lithosphere and the mechanics of slowly accreting plate boundaries. *J. geophys. Res.* **83**, 3955–3970.

Takahashi, E. & Kushiro, I. 1983. Melting of a dry peridotite at high pressures and basalt magma genesis. *Am. Mineral.* **68**, 859–879.

Toramaru, A. & Fujii, N. 1986. Connectivity of melt phase in a partially molten peridotite. *J. geophys. Res.* **91**, 9239–9252.

Tullis, J. & Yund, R. A. 1982. Grain growth kinetics of quartz and calcite aggregates. *J. Geol.* **90**, 301–318.

Twiss, R. J. 1977. Theory and applicability of a recrystallized grain size paleopiezometer. *Pure & Appl. Geophys.* **115**, 227–244.

van der Wal, D., Vissers, R. L. M., Drury, M. R. & Hoogerduijn Strating, E. H. 1992. Oblique fabrics in porphyroclastic Alpine-type peridotites: a shear sense indicator for upper mantle flow. *J. Struct. Geol.* **14**, 839–846.

Volker, J. A. & Upton, B. G. J. 1990. The structure and petrogenesis of the Trallval and Ruinsival areas of the Rhum ultrabasic complex. *Trans. R. Soc. Edin., Earth Sci.* **81**, 69–88.

Waff, H. S. & Bulau, J. R. 1979. Equilibrium fluid distribution in an ultramafic partial melt under hydrostatic stress conditions. *J. geophys. Res.* **84**, 6109–6114.

Williams, H. 1973. Bay of Islands map area, Newfoundland (12G). *Geol. Surv. Can. Pap.* **72-34** (includes map 1355A).

Williams, H. 1975. Structural succession, nomenclature, and interpretation of transported rocks in western Newfoundland. *Can. J. Earth Sci.* **12**, 1874–1894.

Williams, H. & Cawood, P. A. 1989. Geology, Humber Arm Allochthon, Newfoundland. *Geol. Surv. Can., Map* 1678A, scale 1:250,000.